ADVANCED FUNCTIONAL MATERIALS
www.afm-journal.de

www.MaterialsViews.com

# Nickel–Cobalt Layered Double Hydroxide Nanosheets for High-performance Supercapacitor Electrode Materials

*Hao Chen, Linfeng Hu, Min Chen, Yan Yan, and Limin Wu**

**A facile and novel one-step method of growing nickel-cobalt layered double hydroxide (Ni-Co LDH) hybrid films with ultrathin nanosheets and porous nanostructures on nickel foam is presented using cetyltrimethylammonium bromide as nanostructure growth assisting agent but without any adscititious alkali sources and oxidants. As pseudocapacitors, the as-obtained Ni-Co LDH hybrid film-based electrodes display a significantly enhanced specific capacitance (2682 F $g^{-1}$ at 3 A $g^{-1}$, based on active materials) and energy density (77.3 Wh $kg^{-1}$ at 623 W $kg^{-1}$), compared to most previously reported electrodes based on nickel-cobalt oxides/hydroxides. Moreover, the asymmetric supercapacitor, with the Ni-Co LDH hybrid film as the positive electrode material and porous freeze-dried reduced graphene oxide (RGO) as the negative electrode material, exhibits an ultrahigh energy density (188 Wh $kg^{-1}$) at an average power density of 1499 W $kg^{-1}$ based on the mass of active material, which greatly exceeds the energy densities of most previously reported nickel or cobalt oxide/hydroxide-based asymmetric supercapacitors.**

## 1. Introduction

Supercapacitors have drawn great interest in the past decades due to their fast charge and discharge rate, high power density (1–2 orders of magnitude higher than batteries), long cycle lifetime (2–3 orders of magnitude longer than batteries), and high reliability.[1,2]

Currently, most commercial supercapacitor electrode materials are pure carbon-based electric double layer capacitive materials.[3,4] They usually possess good cycle lifetime and high maximum power density, but do not have high enough specific capacitance or energy density to meet the ever-growing need for peak-power assistance in electric vehicles.[5] Compared with pure carbon-based materials, pseudocapacitive materials can obviously enhance the specific capacitance and energy density of supercapacitors by using interfacial reversible faradaic reactions to store energy.[3,6] Moreover, when combined with electric double-layer capacitive materials to construct asymmetric supercapacitors, pseudocapacitive materials can achieve a further enhancement of energy and power density of supercapacitors[4,7,8] Traditional pseudocapacitive materials mainly include typical transitional metal oxides/hydroxides, such as $RuO_2$, $MnO_2$, NiO, $Ni(OH)_2$, $Co_3O_4$, $Co(OH)_2$, $Fe_3O_4$, and their binary systems.[9–15] Recently, metallic layered double hydroxides (LDHs) with a general formula of $[M^{2+}_{1-x}M^{3+}_{x}(OH)_2]^{x+}[A^{n-}_{x/n}\cdot mH_2O]^{x-}$ ($M^{2+}$ and $M^{3+}$, the bivalent and trivalent metal cations, respectively; $A^{n-}$, the charge-balancing anion of valence $n$; $x = M^{3+}/(M^{2+} + M^{3+})$) have attracted increasing interest from both academic and industrial angles due to their wide applications in areas such as catalysis, separation, biotechnology, electrochemistry.[16] Specially, LDHs have exhibited great application potential in supercapacitors.[17–19] For example, Huang et al. fabricated Al-Ni LDH nanosheets on nickel foam by a hydrothermal process.[20] The as-prepared Al-Ni LDH supported on Ni foam as supercapacitor electrode exhibited very high specific capacitance (2123 $F\cdot g^{-1}$ at 1 $A\cdot g^{-1}$) and long cycle life.

In this paper, we present a facile and novel one-step method of growing nickel-cobalt layered double hydroxide (Ni-Co LDH) hybrid films with ultrathin nanosheets and porous nanostructures for supercapacitors. It only involves a simple hydrothermal co-deposition of the precursors of nickel and cobalt hydroxides on nickel foams. Unlike previous synthetic methods of LDHs,[21,22] it needs neither any adscititious alkali sources nor oxidants for producing $OH^-$ ions and trivalent cations, respectively. Accordingly, the as-obtained hybrid films have the following advantages over previous pseudocapacitive materials: (i) The Ni-Co LDH nanosheets align quasi vertically on the nickel surfaces and the resultant well-defined porous nanostructure therefrom allows the easy access of electrolyte to the entire nanosheets. Moreover, no binder is needed, which can prevent the decrease in electrical conductivity caused by the electrical resistance of the binder. (ii) The layered crystal structure of LDHs, made up of positively charged host layers, interlayer charge compensating anions and solvation molecules, can promote the deep ions diffusion among electrode materials for highly efficient utilization of active sites. (iii) The as-obtained single crystalline bimetallic hydroxides possess stronger layered orientation than unitary hydroxides, which can improve the electron transportation from active materials to current collector, and allow nickel and cobalt hydroxides to contribute their double pseudocapacitance more efficiently. The as-obtained Ni-Co LDH hybrid film-based electrodes exhibited significantly

Dr. H. Chen, Dr. L. F. Hu, Dr. M. Chen, Y. Yan, Prof. L. M. Wu
Department of Materials Science and Advanced Materials Laboratory
Fudan University
Shanghai, 200433, China
E-mail: lmw@fudan.edu.cn

DOI: 10.1002/adfm.201301747

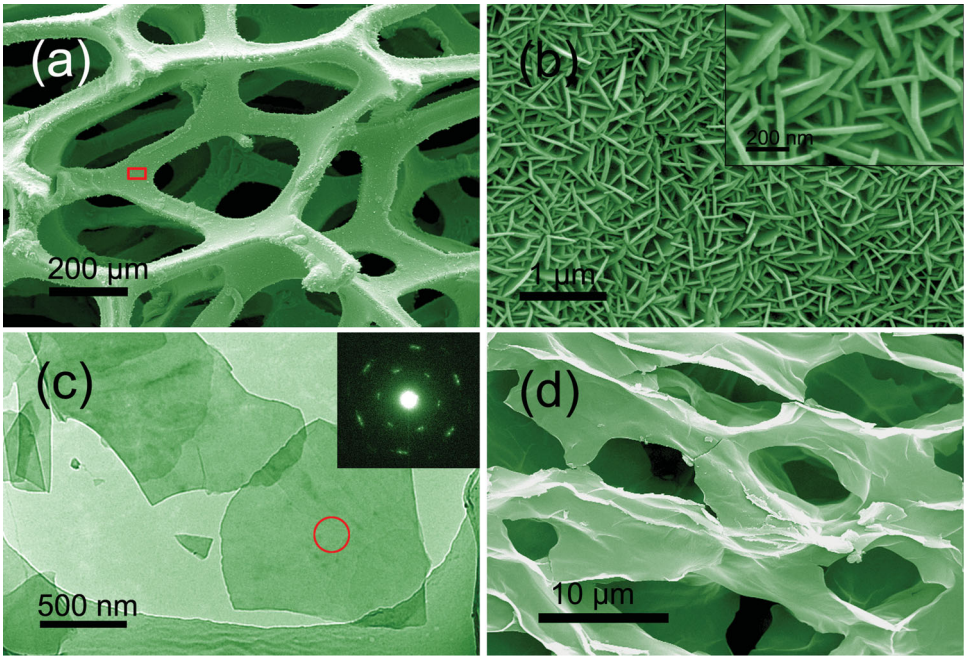


**Figure 1.** Typical SEM images of (a) the hybrid film supported on Ni foam at low-magnification, (b) the hybrid nanosheet at high magnification (red box area in a), the insert is the image at higher-magnification, (c) typical TEM image of the hybrid nanosheets, the insert is the SAED pattern for the circle red area, and (d) typical SEM image of the freeze-dried porous RGO. (Hybrid film was prepared at 6:4 of Ni:Co feeding mole ratio.)

enhanced specific capacitance and energy density (based on active materials) compared to most previously reported electrodes based on nickel-cobalt oxides/hydroxides. In addition, when this Ni-Co LDH hybrid film was used as the positive electrode materials and the porous freeze-dried reduced graphene oxide (RGO) as the negative electrode materials to fabricate the asymmetric supercapacitor, the obtainable highest energy density (based on active materials) has greatly exceeded the energy densities of most previously reported nickel or cobalt oxide/hydroxide based asymmetric supercapacitors and other typical asymmetric supercapacitors.

## 2. Results and Discussion

### 2.1. Fabrication of the Hybrid Film Electrodes

**Figure 1**a shows a typical scanning electron microscope (SEM) image of the as-obtained hybrid film supported on the 3D macroporous nickel foam substrate. 3D structure of nickel foam was well retained after being covered with hybrid film. As shown in Figure 1b, this hybrid film possesses a porous nanostructure composed of around 26 nm thick nanosheets. These nanosheets are intersected and aligned vertically on the nickel foam. This vertical array and the resultant porous nanostructure therefrom facilitates the charge transport and ion diffusion without any blocks of binders. Typical transmission electron microscope (TEM) image of the as-obtained hybrid nanosheet shows a transparent feature (Figure 1c), further indicating its ultrathin nature. The selected-area electron diffraction (SAED) pattern of the hybrid nanosheets reveals hexagonally arranged spots (insert of Figure 1c), confirming the single crystallinity of as-obtained nanosheet and suggesting its relatively good electron transportation ability for supercapacitors. The energy dispersive X-ray spectroscopy (EDX) spectrum (**Figure 2**a) of the selected red area in Figure 1c reveals that the as-obtained single nanosheet mainly contains Ni, Co, O, Br, and Cl elements, except for most of C and Cu signals from the carbon-supported Cu grid, compared with EDX spectrum of hybrid nanosheets supported on nickel foam (Figure S1a in Supporting Information). The Ni:Co ratio of the as-obtained nanosheet can be calculated to be 3.25:1, which is higher than its feeding ratio (6:4). This should be attributed to that the solubility constant ($K_{sp}$) of $Co(OH)_2$ is higher than that of $Ni(OH)_2$.[23]

In the X-ray diffraction (XRD) pattern of the hybrid nanosheets (Figure 2b), the well-defined diffraction peaks observed at $2\theta$ values of 11.1, 22.2, 34.4, and 38.5° can be successfully indexed to (003), (006), (009), and (015) plane reflections of hydrotalcite-like LDH phase.[20] Much clearer diffraction peaks can also be observed for their powder sample. In Ni 2p X-ray photoelectron spectroscopy (XPS) spectrum of hybrid nanosheets (Figure 2c), two obvious shakeup satellites (indicated as "Sat") close to two spin-orbit doublets at 873.3 and 855.6 eV can be identified as Ni $2p_{1/2}$ and Ni $2p_{3/2}$ signals of $Ni^{2+}$, respectively.[24,25] In Co 2p XPS spectrum, the spin-orbit splitting value of Co $2p_{1/2}$ and Co $2p_{3/2}$ reaches 15.2 eV, and the Co $2p_{3/2}$ satellite line intensity is pretty low (Figure 2d), suggesting the co-existence of $Co^{2+}$ and $Co^{3+}$ in the hybrid nanosheets.[21,26] These results indicate that the as-obtained hybrid nanosheets are Ni-Co LDHs,[21] and the $Br^-$ and $Cl^-$ ions have been intercalated into Ni-Co LDHs based on the above EDX result.

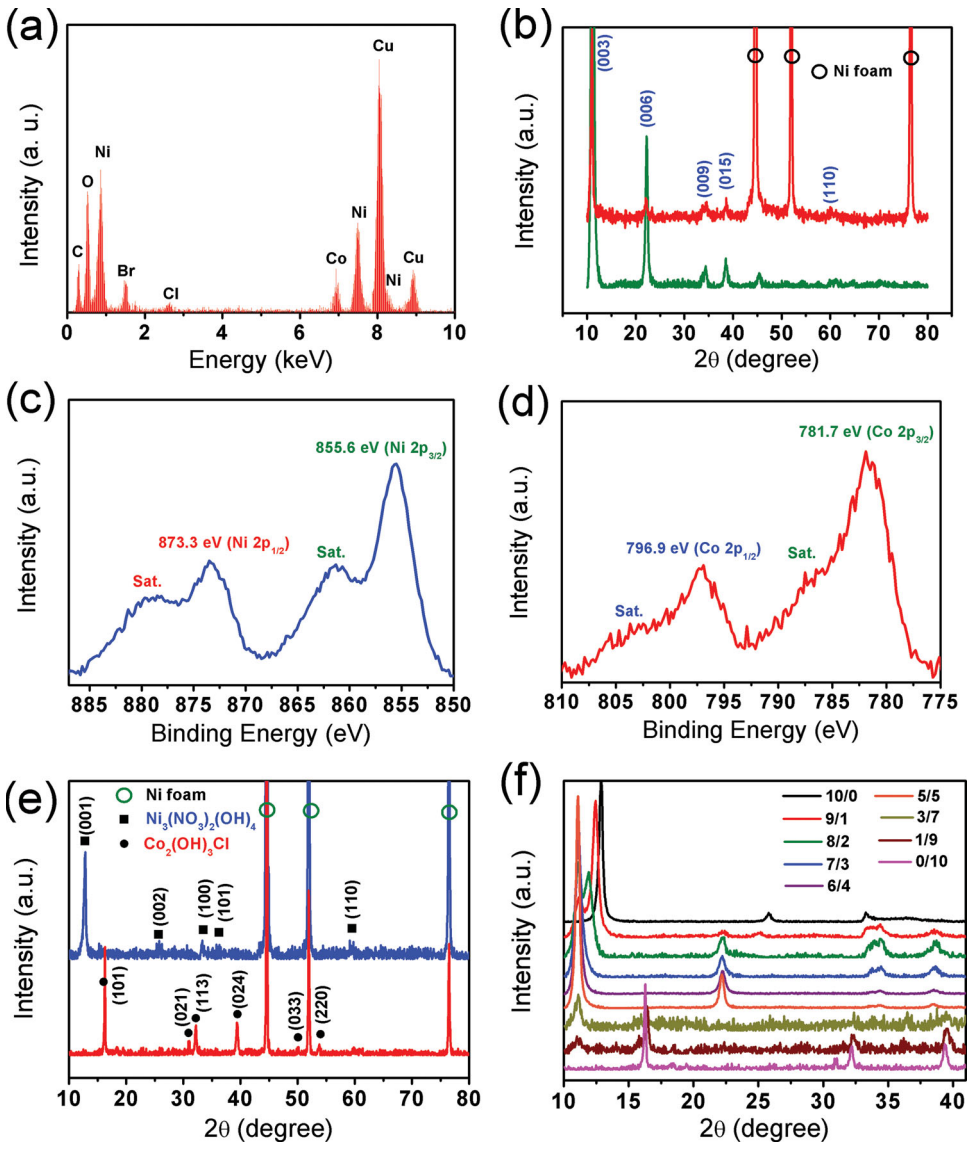


**Figure 2.** (a) Selected-area EDX spectrum of single hybrid nanosheet (red selected area in Figure 1c). XRD patterns of (b) hybrid nanosheets supported on Ni foam (red line) and hybrid nanosheets powder (green line, 6:4 of Ni:Co feeding mole ratio), (e) the unitary nickel hydroxide electrode (blue line) and cobalt hydroxide electrode (red line). (c) Ni 2p XPS and (d) Co 2p XPS spectra of hybrid nanosheets supported on Ni foam (6:4 of Ni:Co feeding mole ratio). (f) XRD patterns of the hybrid nanosheets prepared with different Ni:Co feeding mole ratios (Black line: pure $Ni_3(NO_3)_2(OH)_4$ phase, violet line: pure Ni-Co LDH phase, pink line: pure $Co_2(OH)_3Cl$ phase).

Fourier transform infrared spectroscopy (FTIR) spectrum further illustrates that as-obtained Ni-Co LDH possesses abundant hydrophilic hydroxyl groups (Figure S1b, Supporting Information), which favor its good wettability to electrolyte.

In addition, without $Co^{2+}$ addition, the as-obtained product can be identified as $Ni_3(NO_3)_2(OH)_4$ phase (JCPDS 22–0752) by XRD pattern (Figure 2e), while the product synthesized without $Ni^{2+}$ was found to be pure $Co_2(OH)_3Cl$ phase (JCPDS 73–2134). Moreover, the comparison of XRD patterns of the hybrid nanosheets (Figure 2f) indicates a gradual transformation of crystal structure from $Ni_3(NO_3)_2(OH)_4$ phase to Ni-Co LDH phase and then to $Co_2(OH)_3Cl$ phase, as the feeding Ni:Co mole ratio increased.

The Ni-Co LDH hybrid nanosheets probably formed through a mechanism similar to the preferentially oriented growth of hydrotalcite-like α-$Ni(OH)_2$ nanosheets.[27–30] As illustrated in **Scheme 1**, $Ni^{2+}$ and $Co^{2+}$ first reacted with $OH^-$ to produce nickel and cobalt hydroxide monomers,[27] which precipitated as nuclei and quickly grew into the primary particles. In this process, partial bivalent cobalt was converted to trivalent cobalt by high temperature oxidation, instead of adscititious halogen oxidant.[21,31,32] These primary particles aggregated into chains which partly deposited on the surface of nickel substrate to become the aggregation cores. As the nickel and cobalt (including trivalent cobalt) hydroxide primary particles continued to aggregate, they underwent olation reactions with each

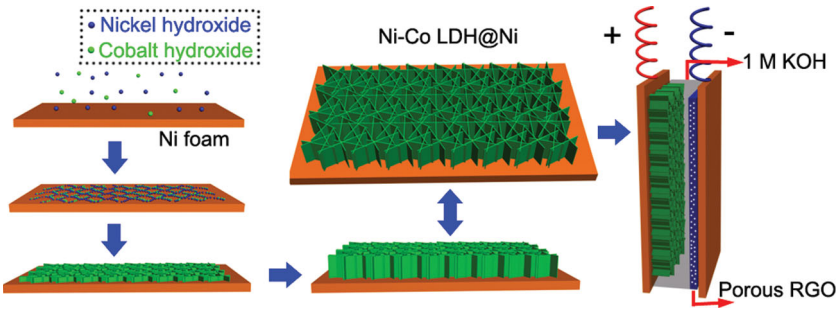


**Scheme 1.** The possible formation mechanism of Ni-Co LDH hybrid films supported on Ni foams and the illustration scheme of the asymmetrical supercapacitors.

other due to random dispersion of nickel and cobalt hydroxide primary particles. And then they began to crystallize and grow along the c-axis, gradually forming a Ni-Co LDH nanosheet layer.[33] Because the aggregation cores might distribute on nickel substrates along different directions, the as-formed Ni-Co LDH hybrid nanosheets were intersected, producing films with highly well-define porous structures. Unlike the methods using adscititious alkali to produce $OH^-$ (**Figures 3**a, b),[21,32] the present process involved the relatively slow redox reaction between solvent and raw material to produce $OH^-$ at high temperatures, which facilitated the relatively slow generation and aggregation of primary particles and relatively fast crystallization for the formation of thinner, larger nanosheets (Figure 1b). In addition, during the hybrid nanosheet growth, surfactant cetyltrimethylammonium bromide (CTAB) might selectively stabilize the exposed planes of nanosheets and finally improved the size uniformity of nanosheets (Figure 1b vs. Figure 3c) through electrostatic interaction between the ionic head-groups of CTAB and the outside $OH^-$ groups of Ni-Co LDH nanosheets.[34,35] And it also made the intercalated $Br^-$ as counteranions of Ni-Co LDH host layers for broadening interlayer spacing (from 0.774 to 0.796 nm) between the neighboring crystal layers of layered crystal structure of Ni-Co LDH,[36,37] which can be reflected by the location of main diffraction peak in XRD patterns (main diffraction peak at lower angle mean larger interlayer spacing, Figure 3d). In this way, the as-obtained hybrid nanosheet-based films enjoyed a well-defined porous nanostructure and good ions access availability.

**Figure 4** shows the images of the as-obtained films as a function of the feeding mole ratios of Ni:Co. Without Co, the as-obtained nickel hydroxide ($Ni_3(NO_3)_2(OH)_4$) film appeared 60 nm thick and only minimally porous (Figure 4a). With the addition of $Co^{2+}$, the mean thickness of the hybrid nanosheets decreased to 50 nm. More pores and crossed sheet-structure appeared at the Ni:Co ratio of 9:1 (Figure 4b). As the concentration of $Co^{2+}$ increased from 8:2 and 7:3 to 6:4, more Co became embedded into Ni-Co LDH nanosheets, and the mean thickness of the Ni-Co LDH nanosheets decreased to 40, 30, and 26 nm, respectively (Figures 4c,d, and Figure 1b). More importantly, incorporation of Co improved the size uniformity of nanosheet and the porous structure of film. This should be attributed to the increasing oriented growth ability and the weakening

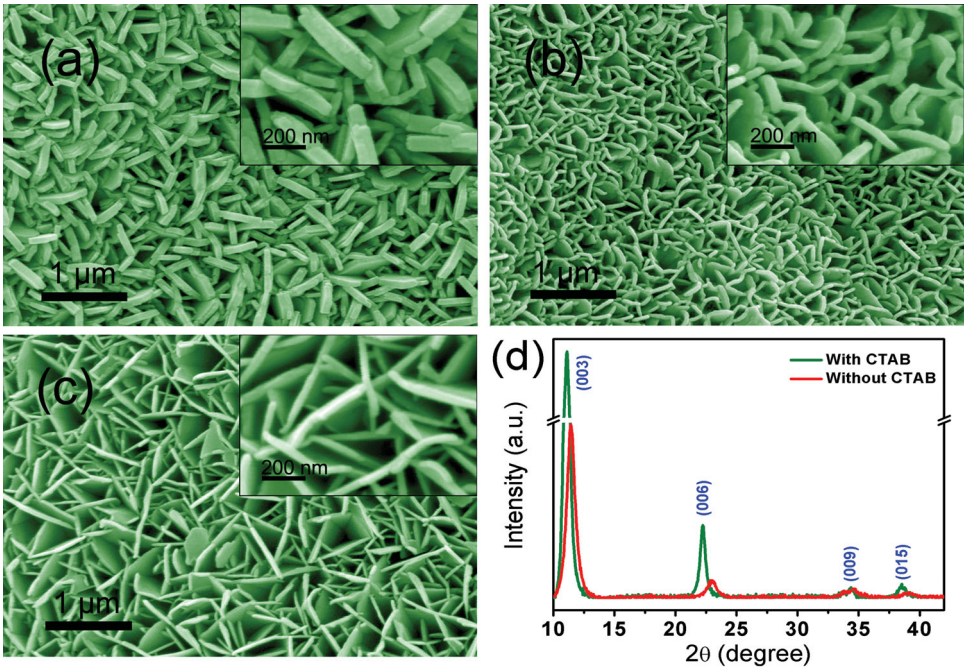


**Figure 3.** SEM images of the as-obtained nanosheets obtained at 6:4 Ni:Co with (a) urea (mean thickness: 65 nm) and (b) hexamine (mean thickness: 40 nm) as adscititious alkali sources. (c) The nanosheets obtained at 6:4 Ni:Co without CTAB (mean thickness: 30 nm). (d) Comparison of XRD patterns of the Ni-Co LDH prepared with and without CTAB.

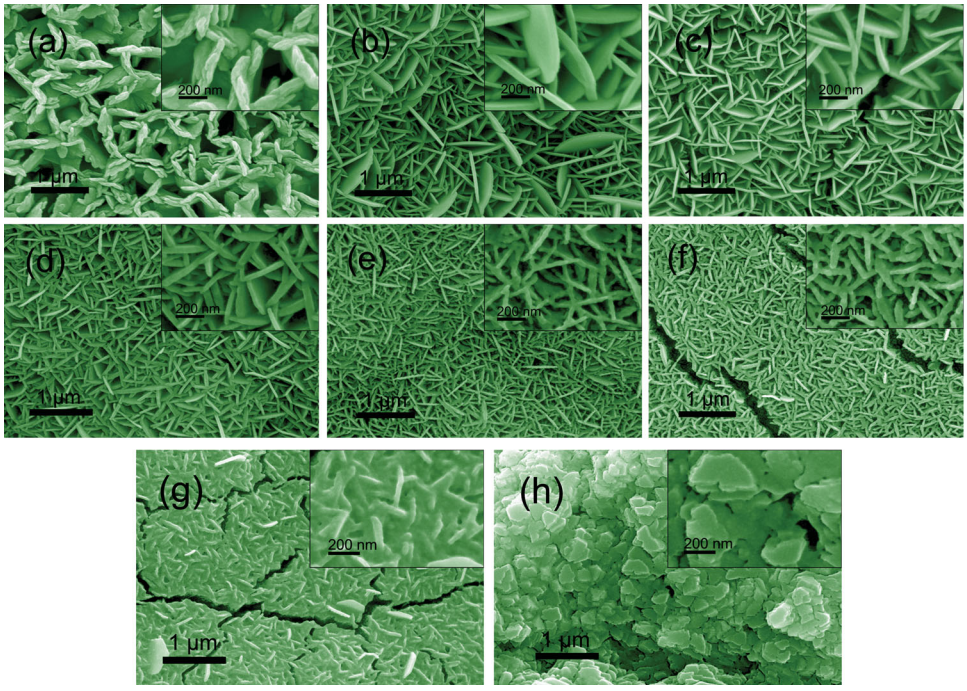


**Figure 4.** SEM images of the as-obtained nanosheets obtained at different Ni:Co feeding mole ratios and with various nanosheet thickness: (a) 10:0, 60 nm, (b) 9:1, 50 nm, (c) 8:2, 40 nm, (d) 7:3, 30 nm, (e) 5:5, 23 nm, (f) 3:7, 30 nm, (g) 1:9, (h) 0:10.

self-aggregation of nanosheets made through the incorporation of cobalt. As indicated in XRD results above (Figure 2f), the presence of cobalt ion can induce active material crystal transition from $Ni_3(NO_3)_2(OH)_4$ to Ni-Co LDH, which has highly oriented growth ability.[21] Moreover, trivalent cations isomorphically replaced some of the bivalent cation sites in formed layered double hydroxides, inducing excessive positive electric charge to the host sheets,[32] which can depress the excessive self-aggregation of double hydroxide layers by electrostatic interaction. More Co addition decreased the thickness of Ni-Co LDH nanosheets, yet increased the size of particles attached to the surface of Ni-Co LDH nanosheets (Figure 4e–g). This may be resulted from the formation and growth of new cobalt hydroxide ($Co_2(OH)_3Cl$) phase besides LDH phase (Figure 2f). The pure cobalt hydroxide film ($Co_2(OH)_3Cl$) without $Ni^{2+}$ showed the aggregation of massive particles, as shown in Figure 4h.

### 2.2. Electrochemical Properties of Hybrid Film Electrodes

The typical cyclic voltammetry (CV) curve (**Figure 5**a) of the as-obtained hybrid film exhibits a pair of well-defined redox peaks within 0.0–0.5 V. This indicates the strong pseudocapacitive nature of the as-obtained electrodes.[38,39] The comparison of CV curve average areas further indicates that the as-obtained hybrid film-electrode possesses a significantly higher specific capacitance than unitary nickel hydroxide or cobalt hydroxide electrodes.[40,41] This can be attributed to the synergistic effects of the Ni-Co LDH hybrid nanostructures as follows: (i) The as-obtained hybrid film was composed of much thinner nanosheets with better-defined porous nanostructures than pure nickel hydroxide or cobalt hydroxide films. This can promote the electrolyte access and the exposure of active sites to electrolyte. (ii) Compared with $Ni_3(NO_3)_2(OH)_4$ or $Co_2(OH)_3Cl$ phases of unitary component electrode, Ni-Co LDH phase of the hybrid nanosheets owned the layered crystal structure with enlarged interlayer spacing (Figure 2f), which can enhance the ions diffusion within active materials. (iii) Ni-Co LDH with highly oriented layered single crystal structure can improve the electron transportation from active materials to the current collector, which can be confirmed by the decreasing equivalent series resistance (Figure 5b). The galvanostatic charge-discharge curves of this hybrid film-based electrode at different current densities (Figure 5c), displayed a typical pseudocapacitive behavior.

Figure 5d demonstrates the $C_s$ of the hybrid film-electrodes at various Ni:Co feeding mole ratios. As more cobalt was embedded, $C_s$ increased. However, too much cobalt, such as 5:5, 3:7 and 1:9 of mole ratios for Ni:Co, caused a decreasing $C_s$ due to the increasing ratio of $Co_2(OH)_3Cl$ (lower $C_s$). This $C_s$ variation could be also well reflected by the gradual changes of crystal structure and morphology of hybrid films at various Ni:Co feeding mole ratios (Figures 2f and 4). The thinner nanosheets with pure LDH phase seemed to be more effective for contributing pseudocapacitance. The hybrid film formed at 6:4 of Ni:Co showed the highest $C_s$ values, at 2682, 2580, 2435, 2339, 2228, 1977, and 1706 F $g^{-1}$ at current densities of 3, 4, 6, 8, 10, 15, and 20 A $g^{-1}$, respectively, based on active materials. The highest $C_s$ (2682 F $g^{-1}$ at 3 A $g^{-1}$) was considerably higher than the specific capacitances of most previously reported nickel-cobalt oxide/hydroxide composite based pseudocapacitive materials (Table S1, Supporting Information). This high

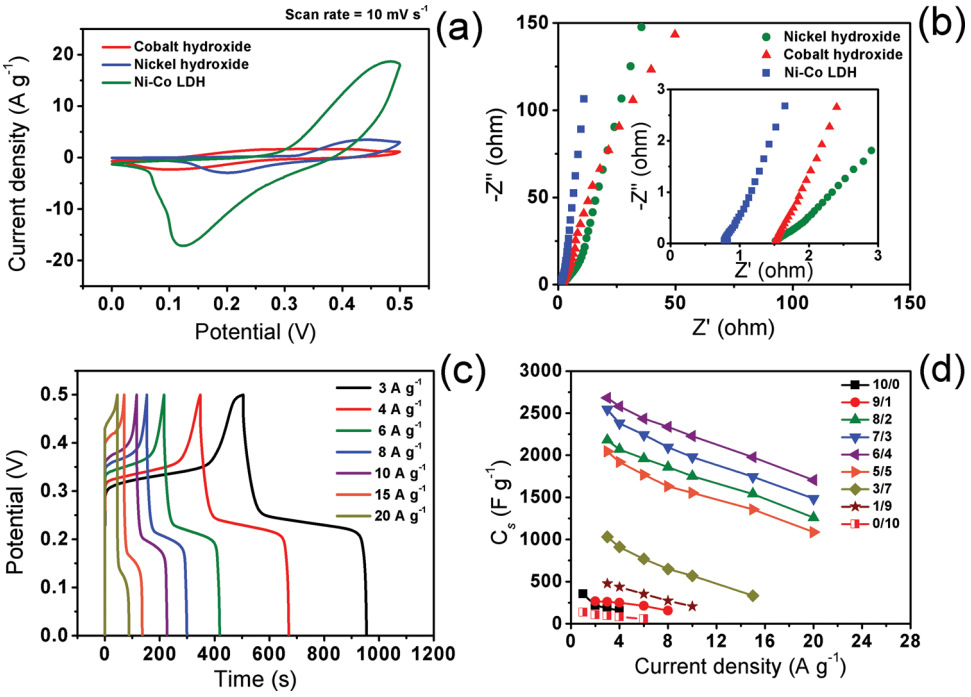


**Figure 5.** (a) Comparison of CV curves of the Ni-Co LDH hybrid-, nickel hydroxide-, and cobalt hydroxide- electrodes at a scan rate of 10 mV $s^{-1}$. (b) Comparison of Nyquist plots of Ni-Co LDH hybrid-, nickel hydroxide-, and cobalt hydroxide- based electrodes. (c) Galvanostatic charge-discharge curves of Ni-Co LDH hybrid electrode at different current densities (6:4 of Ni:Co feeding mole ratio). (d) Comparison of $C_s$ of the Ni-Co LDH hybrid electrodes prepared with different Ni:Co feeding mole ratios.

$C_s$ should be attributed by the unique nanostructure features of the as-obtained Ni-Co LDH hybrid films: highly oriented layered single crystal thin nanosheets aligning quasi vertically on the nickel foam and the resultant well-defined porous nanostructure therefrom. The comparison of $C_s$ of the hybrid film-electrodes prepared with different alkali sources indicates our synthesis method (redox reaction for producing alkaline environment) can significantly enhance the pseudocapacitance of the as-obtained Ni-Co LDH (Figure S2a, Supporting Information). In addition, a visible decrease in $C_s$ can be found when CTAB was removed in the preparation procedure (Figure S2b, Supporting Information), indicating that CTAB also play an important role in synthesizing Ni-Co LDH with high $C_s$.

Based on the as-obtained $C_s$ values, the energy and power densities of the as-obtained hybrid film-electrodes at a 6:4 Ni:Co ratio can be calculated, and are shown in **Figure 6**a. Their energy and power densities are higher than those of unitary nickel hydroxide and cobalt hydroxide electrodes. And the maximum energy density (77.3 Wh $kg^{-1}$ at 623 W $kg^{-1}$) based on active materials was also found to greatly exceed those of most reported nickel-cobalt oxide/hydroxide composite based pseudocapacitive materials (Table S1, Supporting Information).

### 2.3. Electrochemical Properties of Ni-Co LDH Based Asymmetric Supercapacitor

To further investigate the application of the as-fabricated Ni-Co LDH in asymmetric supercapacitors, we also measured the electrochemical properties of the porous freeze-dried RGO (a potential negative material). The as-obtained RGO holds three-dimensional porous feature (Figure 1d), and displays excellent electric double-layer capacitance property at −1.0 to 0.0 V (Figure 6b). The $C_s$ of RGO-electrode can be calculated from its galvanostatic charge-discharge curves (Figure 6c) and reach up to 281 F $g^{-1}$ at 0.5 A $g^{-1}$ (Figure 6d), which is comparable to those of the previously reported graphene based supercapacitors.[7,42]

Due to the excellent capacitance properties of the as-obtained Ni-Co LDH (at 0.0–0.5 V) and RGO (at −1.0–0.0 V), we further used the as-obtained Ni-Co LDH (prepared with 6:4 of Ni:Co feeding mole ratio) as the positive electrode materials and the RGO as the negative electrode materials to successfully fabricate an asymmetric supercapacitor (Ni-Co LDH//RGO), as illustrated in Scheme 1. Its CV curve exhibits double contribution of electric double-layer capacitance and pseudocapacitance at 0–1.6 V (**Figure 7**a). The $C_s$ of Ni-Co LDH//RGO was calculated based on active materials, as shown in Figure 7c, from its galvanostatic charge-discharge curves (Figure 7b). Based on these $C_s$ values, the energy densities of the Ni-Co LDH//RGO can be further calculated to be 188, 141, 105, 78.5, 61.2, and 21.8 Wh $kg^{-1}$ at average power densities of 1499, 2797, 3927, 4881, 5593, and 7324 W $kg^{-1}$, respectively. Compared with individual Ni-Co LDH and RGO, the Ni-Co LDH//RGO exhibits further enhancement in both energy density and power density (Figure 6a). The obtainable highest energy density (188 Wh $kg^{-1}$ at 1499 W $kg^{-1}$) based on active materials has tremendously surpassed those of most nickel or cobalt oxides/hydroxides and other typical

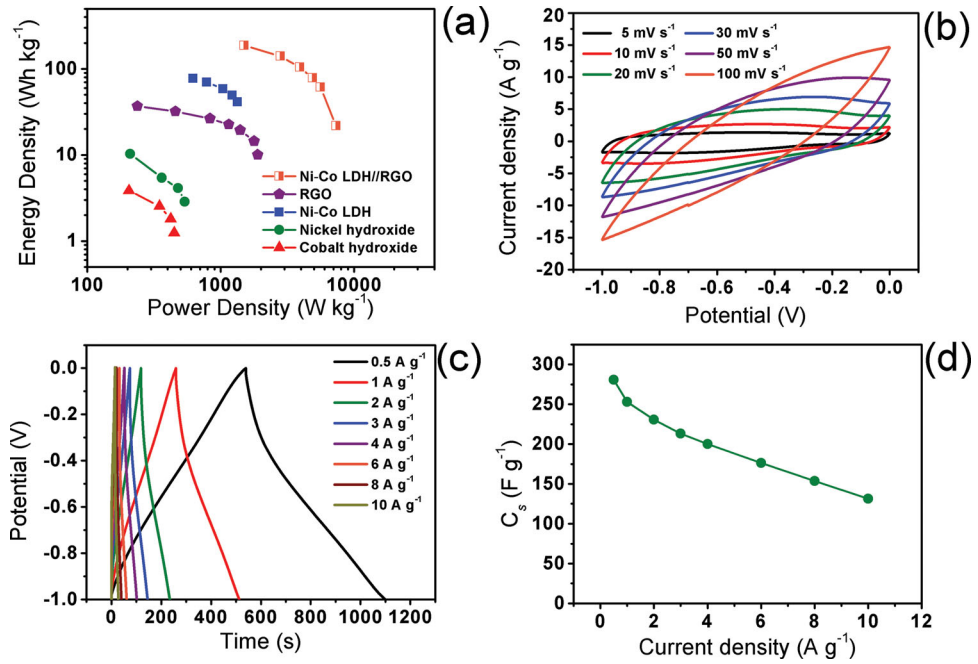


**Figure 6.** (a) Comparison of energy density vs. power density curves of the Ni-Co LDH hybrid-, nickel hydroxide-, cobalt hydroxide-, RGO- electrodes and the Ni-Co LDH//RGO asymmetric supercapacitor. (b) CV curves of the freeze-dried RGO electrode at different scan rates. (c) Galvanostatic charge-discharge curves and (d) $C_s$ of RGO electrode at different current densities.

materials based asymmetric supercapacitors (Table S2, Supporting Information). This ultrahigh energy desity should benefit from the high energy contribution of Ni-Co LDH and the enough power supportion of RGO. We also used galvanostatic charge-discharge measurement to evaluate the durability of the as-fabricated asymmetric supercapacitor. As shown in Figure 7d, the as-obtained asymmetric supercapacitor can retain about 82% of its original capacitance after 5000 cycles, which is comparable to those of some other asymmetric supercapacitors.[7,43]

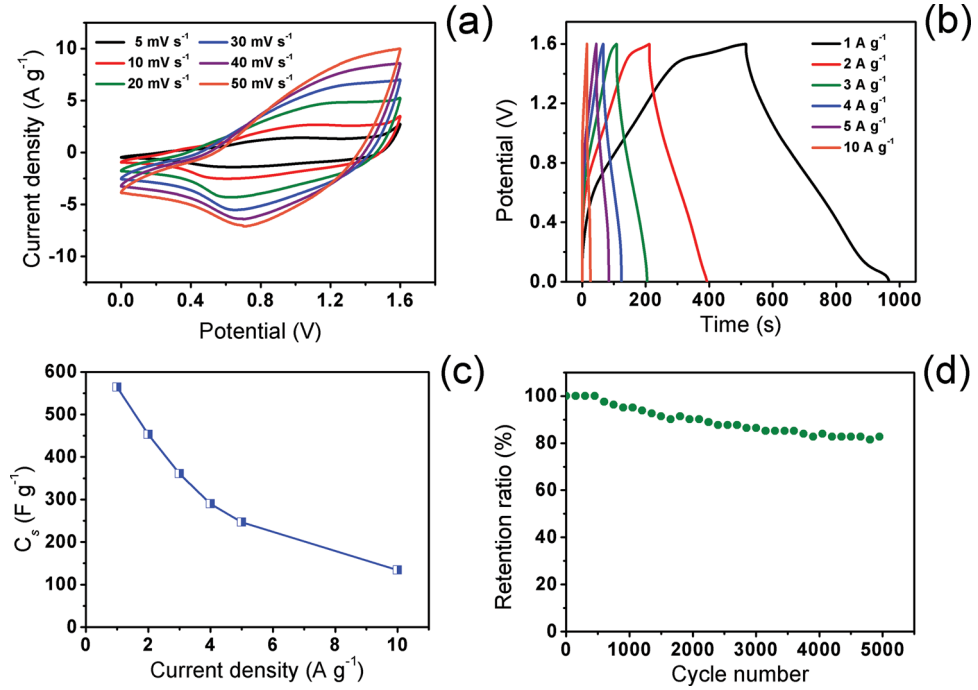


**Figure 7.** (a) CV curves of the Ni-Co LDH//RGO asymmetric supercapacitor at different scan rates. (b) Galvanostatic charge-discharge curves and (c) $C_s$ of Ni-Co LDH//RGO asymmetric supercapacitor at different current densities. (d) Cycling performance of the Ni-Co LDH//RGO asymmetric supercapacitor at a current density of 5 A $g^{-1}$.

## 3. Conclusion

Highly porous hybrid films composed of ultrathin Ni-Co LDH hybrid nanosheets supported on a three-dimensional macroporous nickel foam have been successfully fabricated using a facile one-step hydrothermal co-deposition method using CTAB as the nanostructure growth assisting agent but without any adscititious alkali sources and oxidants. Due to the highly oriented layered single crystal structure and ultrathin nature of hybrid nanosheets as well as the well-define porous nanostructure, the electrodes based on the as-obtained Ni-Co LDH hybrid films exhibited ultrahigh specific capacitance (2682 F $g^{-1}$ at 3 A $g^{-1}$) and energy density (77.3 Wh $kg^{-1}$ at 623 W $kg^{-1}$), based on active materials. Both values were obviously higher than those of most previously reported electrodes based on nickel-cobalt oxides/hydroxides. In addition, the energy density (188 Wh $kg^{-1}$ at 1499 W $kg^{-1}$, based on active materials) of the as-obtained Ni-Co LDH based asymmetric supercapacitor has significantly exceeded those of most previously reported nickel or cobalt oxide/hydroxide-based asymmetric supercapacitors and other typical asymmetric supercapacitors. This suggestes that the as-prepared Ni-Co LDH hybrid films are promising electrode materials to fabricate high performance supercapacitor products by further optimized capsulation. Moreover, this method can be extended to synthesize other bimetallic LDHs with high electrochemical activity for application in supercapacitors, sensors, catalysis, and so on.

## 4. Experimental Section

*Fabrication of Hybrid Film-based Electrodes*: The hybrid electrode material was prepared by a simple one-step process as follows: Typically, nickel foam (10 mm × 50 mm × 0.1 mm, 110 ppi (pores per inch), 320 g $m^{-2}$) was pretreated successively with acetone, 2 M HCl solution, deionized water, and absolute ethanol, each for 15 min, to ensure a clean surface. The cleaned nickel foam was then partially immersed in a 100 mL Teflon autoclave with a homogeneous solution of $Ni(NO_3)_2{\cdot}6H_2O$ (0.21 mmol), $CoCl_2{\cdot}6H_2O$ (0.14 mmol), CTAB (0.50 g), $H_2O$ (3.0 g), and methanol (12.0 g), followed by heating the autoclave in an oven at 180 °C for 24 h to allow the growth of Ni-Co LDH hybrid nanosheets on Ni foam, through the following reactions: (i) Methanol and $NO_3^-$ underwent a redox reaction releasing hydroxyl ions at 180 °C: $4CH_3OH + NO_3^- \rightarrow 4HCHO + NH_3 + OH^- + 2H_2O$;[44,45] (ii) The $Ni^{2+}$ and $Co^{2+}$ ions reacted with $OH^-$ ions to form nickel and cobalt hydroxide monomers; (iii) Partial bivalent cobalt was converted to trivalent cobalt upon reaction with oxygen (from dissolved air) at high temperatures; (iv) nickel and cobalt (including trivalent cobalt) hydroxide monomers were converted to Ni-Co LDH by olation reactions and crystallization. The nickel foam substrate, covered with nanosheets, was washed with $H_2O$ and ethanol to remove surface ions and molecules using an ultrasonic bath cleaner, and then dried at 80 °C for 12 h to remove the adsorbed solvents. For the sake of comparison, the hybrid nanosheets with urea and hexamine as adscititious alkali sources, or without CTAB, or with different Ni:Co feeding mole ratios were also fabricated by the same process. The mass of the nanosheets on Ni foam was determined by subtracting the weight before deposition from the weight after deposition. The loading densities of active materials were about 3 mg $cm^{-2}$ for all electrodes.

*Fabrication of RGO Electrodes*: Graphene oxide (GO) was firstly prepared by our previously reported method.[46] The GO suspension was then freeze-dried overnight to obtain the freeze-dried GO. This product was reduced to the freeze-dried reduced graphene oxide (RGO) by 150 °C thermal treatment for 1 h at vacuum.[47] Due to thermal treatment of solid samples, the formed three-dimensional porous structure of the freeze-dried GO was retained. RGO electrodes was fabricated using the method as follows: a mixture of RGO, 23 wt% of acetylene black (as an electrical conductor), 5 wt% of polytetrafluoroethylene (as a binder), and a small amount of ethanol was prepared by milling to produce a homogeneous paste. This paste was then pressed onto nickel foam current-collectors to produce RGO electrode.

*Characterization*: The morphologies were observed by scanning electron microscope (SEM, S-4800, Hitachi). The SAED pattern and TEM images were obtained on a Philips CM200FEG field emission microscope. The crystalline structure was characterized by XRD patterns recorded in a Rigaku D/max-kA diffractometer with Cu Kα radiation. X-ray photoelectron spectroscopy (XPS, PHI 5000C ESCA System) and Energy-dispersive X-ray spectroscopy (EDX, TSL, AMETEK) measurements were employed to investigate the elemental compositions of the samples. Fourier transform infrared spectroscopy (FTIR, Nicolet Nexus 470) measurement was used to characterize the functional groups of the samples.

*Electrochemical Measurement*: The electrochemical properties of the as-obtained hybrid film- and the RGO- based electrodes were investigated under a three-electrode cell configuration at 25 °C. The nickel foam supporting hybrid nanosheets were acted directly as the working electrodes, which were soaked in a 1 M KOH solution and degassed in a vacuum for 5 h before the electrochemical test. Platinum foil and a saturated calomel electrode (SCE) were used as the counter and reference electrodes, respectively. The electrochemical properties of asymmetric supercapacitor were investigated under a two-electrode cell configuration with Ni-Co LDH hybrid film as the positive electrode and RGO as the negative electrode in 1 M KOH electrolyte solution. The cyclic voltammetry (CV), galvanostatic charge-discharge, and electrochemical impedance spectroscopy (EIS) measurements were conducted on a CHI 660B electrochemical workstation (Shanghai CH Instrument Company, China). The $C_s$ of hybrid film-electrodes at various Ni:Co feeding mole ratios and RGO electrode were calculated from galvanostatic charge-discharge curves as follows: $C_s = I \times \Delta t/(\Delta V \times m)$, where $C_s$ ($F{\cdot}g^{-1}$) is the specific capacitance, $I$ (A) is the discharge current, $\Delta t$ (s) is the discharge time, $\Delta V$ (V) is the potential change during the discharge, and $m$ (g) is the mass of the active material in the electrode. The $C_s$ of asymmetric supercapacitor was calculated from galvanostatic charge-discharge curves as follows: $C_s = 4 \times I \times \Delta t/(\Delta V \times m')$, where $m'$ (g) is the total mass of the active material in the positive and negative electrodes. The energy and power densities of the hybrid film-, RGO- based electrodes, and the asymmetric supercapacitor were calculated as follows:[8,48,49] $E = 0.5 \times C \times V^2$, $P_{ave} = E/\Delta t$, where $E$ (Wh $kg^{-1}$) is the energy density, $V$ (V) is the cell voltage excluding IR drop, $P_{ave}$ (W $kg^{-1}$) is the average power density, and $\Delta t$ (s) is the discharge time.

## Supporting Information

Supporting Information is available from the Wiley Online Library or from the author.

## Acknowledgements

Financial supports were received from the National Natural Science Foundation of China (Grants 51133001, 21074023, 21374018 and 51372040), National 863 Foundation, Doctorate Foundation of Ministry of Education of China (20110071130002), Science and Technology Foundation of Shanghai (12nm0503600, 13JC1407800, 12PJ1400300) and Innovation Program of Shanghai Municipal Education Commission (14ZZ003).

Received: May 22, 2013
Revised: July 10, 2013
Published online: September 23, 2013

[1] M. Winter, R. J. Brodd, *Chem. Rev.* **2004**, *104*, 4245.
[2] A. Burke, *J. Power Sources* **2000**, *91*, 37.
[3] P. Simon, Y. Gogotsi, *Nat. Mater.* **2008**, *7*, 845.
[4] P. C. Chen, G. Shen, Y. Shi, H. Chen, C. Zhou, *ACS Nano* **2010**, *4*, 4403.
[5] J. Huang, B. G. Sumpter, V. Meunier, *Angew. Chem. Int. Ed.* **2008**, *47*, 520.
[6] M. Inagaki, H. Konno, O. Tanaike, *J. Power Sources* **2010**, *195*, 7880.
[7] J. Yan, Z. Fan, W. Sun, G. Ning, T. Wei, Q. Zhang, R. Zhang, L. Zhi, F. Wei, *Adv. Funct. Mater.* **2012**, *22*, 2632.
[8] L. Bao, X. Li, *Adv. Mater.* **2012**, *24*, 3246.
[9] X. Y. Lang, A. Hirata, T. Fujita, M. W. Chen, *Nat. Nanotechnol.* **2011**, *6*, 232.
[10] J. Jiang, Y. Li, J. Liu, X. Huang, C. Yuan, X. W. Lou, *Adv. Mater.* **2012**, *24*, 5166.
[11] C. Yuan, L. Yang, L. Hou, L. Shen, X. Zhang, X. W. Lou, *Energy Environ. Sci.* **2012**, *5*, 7883.
[12] L. Yang, S. Cheng, Y. Ding, X. Zhu, Z. L. Wang, M. Liu, *Nano Lett.* **2012**, *12*, 321.
[13] X. Xia, J. Tu, Y. Zhang, X. Wang, C. Gu, X.-b. Zhao, H. J. Fan, *ACS Nano* **2012**, *6*, 5531.
[14] C. Guan, X. Li, Z. Wang, X. Cao, C. Soci, H. Zhang, H. J. Fan, *Adv. Mater.* **2012**, *24*, 4186.
[15] H. Chen, L. Hu, Y. Yan, R. Che, M. Chen, L. Wu, *Adv. Energy Mater.* **2013**, DOI: 10.1002/aenm.201300580.
[16] Q. Wang, D. O'Hare, *Chem. Rev.* **2012**, *112*, 4124.
[17] L. Wang, D. Wang, X. Y. Dong, Z. J. Zhang, X. F. Pei, X. J. Chen, B. Chen, J. Jin, *Chem. Commun.* **2011**, *47*, 3556.
[18] Z. Gao, J. Wang, Z. Li, W. Yang, B. Wang, M. Hou, Y. He, Q. Liu, T. Mann, P. Yang, M. Zhang, L. Liu, *Chem. Mater.* **2011**, *23*, 3509.
[19] Z.-A. Hu, Y.-L. Xie, Y.-M. Wang, H.-Y. Wu, Y.-Y. Yang, Z.-Y. Zhang, *Electrochim. Acta* **2009**, *54*, 2737.
[20] J. Huang, T. Lei, X. Wei, X. Liu, T. Liu, D. Cao, J. Yin, G. Wang, *J. Power Sources* **2013**, *232*, 370.
[21] J. Liang, R. Ma, N. Iyi, Y. Ebina, K. Takada, T. Sasaki, *Chem. Mater.* **2009**, *22*, 371.
[22] R. Ma, K. Takada, K. Fukuda, N. Iyi, Y. Bando, T. Sasaki, *Angew. Chem. Int. Ed.* **2008**, *47*, 86.
[23] Ö. Yavuz, Y. Altunkaynak, F. Güzel, *Water Res.* **2003**, *37*, 948.
[24] J. W. Lee, T. Ahn, D. Soundararajan, J. M. Ko, J.-D. Kim, *Chem. Commun.* **2011**, *47*, 6305.
[25] N. S. McIntyre, M. G. Cook, *Anal. Chem.* **1975**, *47*, 2208.
[26] R. Ma, J. Liang, K. Takada, T. Sasaki, *J. Am. Chem. Soc.* **2011**, *133*, 613.
[27] G. J. d. A. A. Soler-Illia, M. Jobbágy, A. E. Regazzoni, M. A. Blesa, *Chem. Mater.* **1999**, *11*, 3140.
[28] L. Xu, Y.-S. Ding, C.-H. Chen, L. Zhao, C. Rimkus, R. Joesten, S. L. Suib, *Chem. Mater.* **2007**, *20*, 308.
[29] R. L. Penn, *J. Phys. Chem. B* **2004**, *108*, 12707.
[30] C. Burda, X. Chen, R. Narayanan, M. A. El-Sayed, *Chem. Rev.* **2005**, *105*, 1025.
[31] R. B. Rakhi, W. Chen, D. Cha, H. N. Alshareef, *Nano Lett.* **2012**, *12*, 2559.
[32] R. Ma, J. Liang, X. Liu, T. Sasaki, *J. Am. Chem. Soc.* **2012**, *134*, 19915.
[33] J. W. Lee, J. M. Ko, J.-D. Kim, *J. Phys. Chem. C* **2011**, *115*, 19445.
[34] M. A. Kiani, M. F. Mousavi, S. Ghasemi, *J. Power Sources* **2010**, *195*, 5794.
[35] N. Zhao, L. Qi, *Adv. Mater.* **2006**, *18*, 359.
[36] L. Lv, Y. Wang, M. Wei, J. Cheng, *J. Hazard. Mater.* **2008**, *152*, 1130.
[37] F. Cavani, F. Trifirò, A. Vaccari, *Catal. Today* **1991**, *11*, 173.
[38] U. M. Patil, K. V. Gurav, V. J. Fulari, C. D. Lokhande, O. S. Joo, *J. Power Sources* **2009**, *188*, 338.
[39] G. X. Pan, X. Xia, F. Cao, P. S. Tang, H. F. Chen, *Electrochim. Acta* **2012**, *63*, 335.
[40] J. Zhu, S. Chen, H. Zhou, X. Wang, *Nano Res.* **2012**, *5*, 11.
[41] V. Srinivasan, J. W. Weidner, *J. Power Sources* **2002**, *108*, 15.
[42] Z.-S. Wu, A. Winter, L. Chen, Y. Sun, A. Turchanin, X. Feng, K. Müllen, *Adv. Mater.* **2012**, *24*, 5130.
[43] Z. Tang, C.-h. Tang, H. Gong, *Adv. Funct. Mater.* **2012**, *22*, 1272.
[44] Y. Ren, L. Gao, *J. Am. Ceram. Soc.* **2010**, *93*, 3560.
[45] X. Sun, X. Qiu, L. Li, G. Li, *Inorg. Chem.* **2008**, *47*, 4146.
[46] Z. Tang, H. Chen, X. Chen, L. Wu, X. Yu, *J. Am. Chem. Soc.* **2012**, *134*, 5464.
[47] H. Chen, S. Zhou, M. Chen, L. Wu, *J. Mater. Chem.* **2012**, *22*, 25207.
[48] Z. Fan, J. Yan, T. Wei, L. Zhi, G. Ning, T. Li, F. Wei, *Adv. Funct. Mater.* **2011**, *21*, 2366.
[49] G. Yu, L. Hu, M. Vosgueritchian, H. Wang, X. Xie, J. R. McDonough, X. Cui, Y. Cui, Z. Bao, *Nano Lett.* **2011**, *11*, 2905.